Electronic Supplementary Material (ESI) for Nanoscale.
This journal is © The Royal Society of Chemistry 2020

Homogeneous nucleation of Li_2O_2 under Li-O_2 battery discharge

Tatiana Zakharchenko,[a,b] Artem Sergeev,[b] Alexander Bashkirov,[a] Polina Neklyudova,[c] Antonio Cervellino,[d] Daniil Itkis,[a,b] Lada V. Yashina[a,b,*]

a) N.N. Semenov Federal Research Center for Chemical Physics, Kosygina Street 4 Building 1, 119991 Moscow, Russia

b) Lomonosov Moscow State University, Leninskie gory 1/3, 119991 Moscow, Russia.

c) Institute of Nanotechnology of Microelectronics RAS, Nagatinskaya str., 16A/11, 115487 Moscow, Russia

d) Paul Scherrer Institute, Forschungsstrasse 111, 5232, Villigen, Switzerland

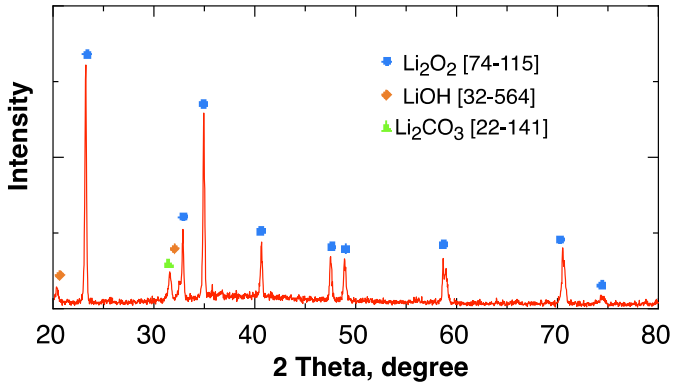

Figure S1. XRD pattern of synthesized Li_2O_2. Numbers in brackets according to PDF-2 database (ICDD).

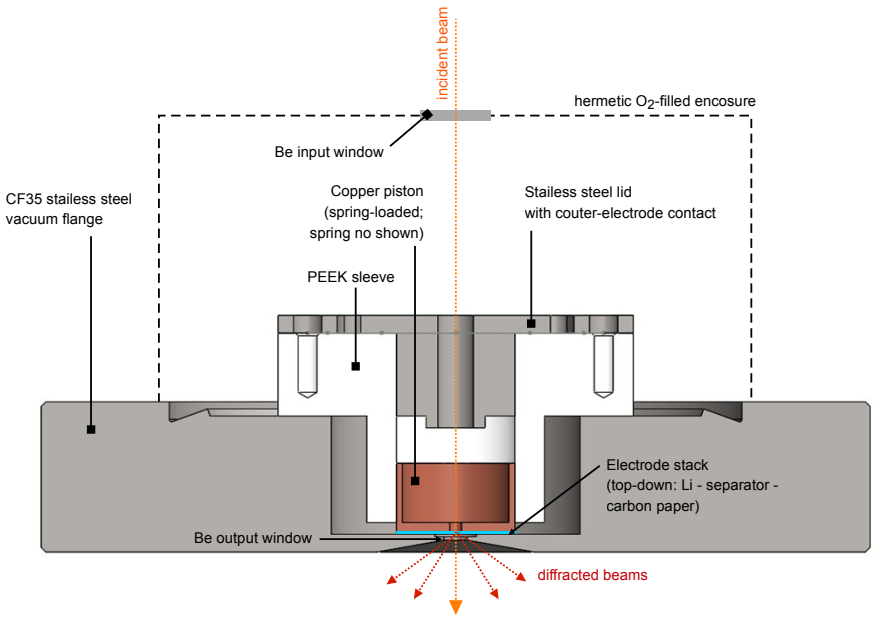

Figure S2. A sketch of the cell used for *operando* XRD studies. Cell construction is similar to used in Ref.[1].

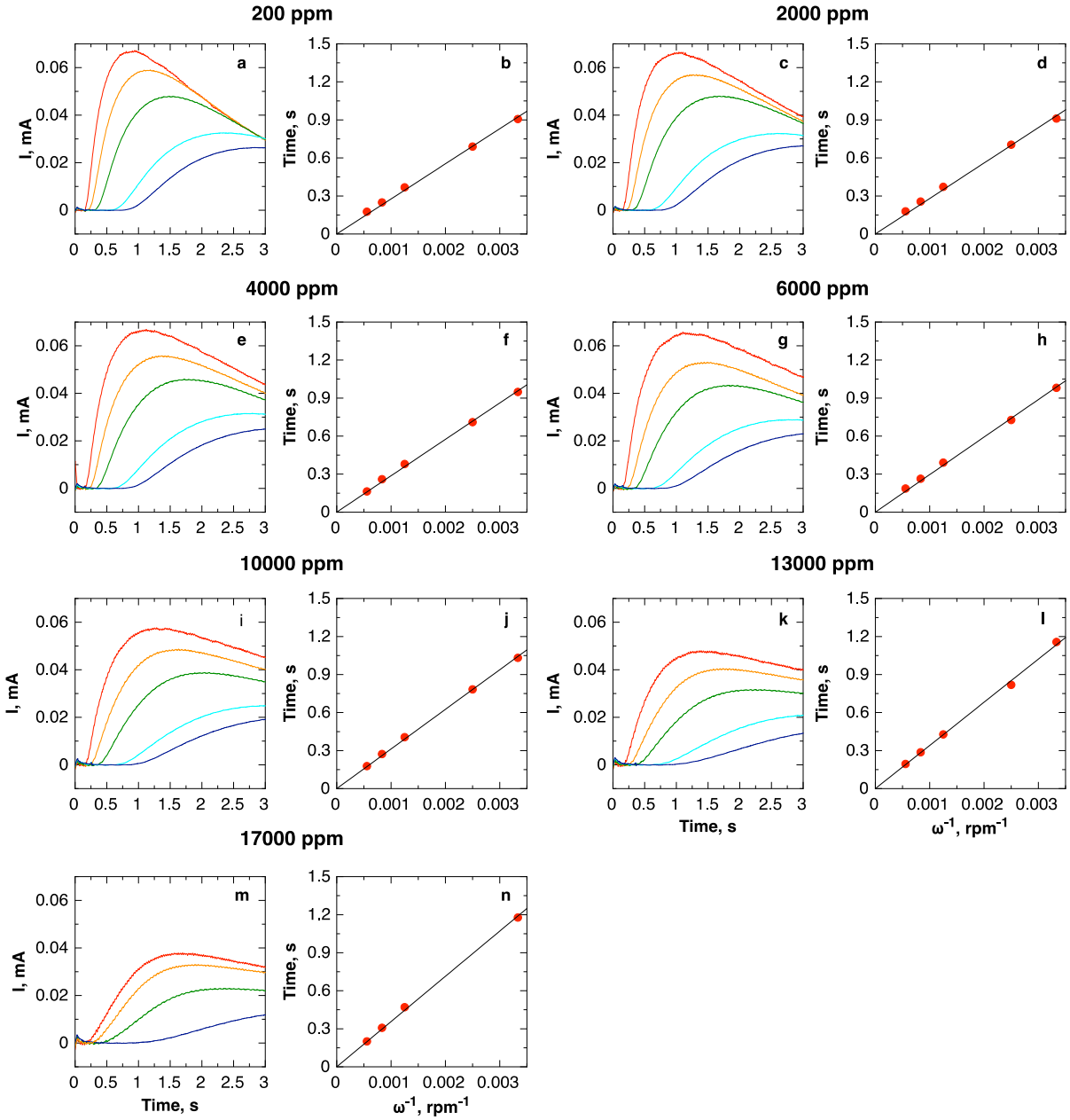

Figure S3. Capacitively corrected ring current time transients registered after disk potential step from -0.8 to -1.3 V vs Ag^+/Ag in electrolyte containing app. 200 (a), 2000 (c), 4000 (e), 6000 (g), 10000 (i), 13000 (k), 17000 (m) ppm of water and corresponding relations between the inverse of rotation speed and transient time (b, d, f, h, i, l, n). Note that fitted lines forced to passed through the origin of the axes (0,0).

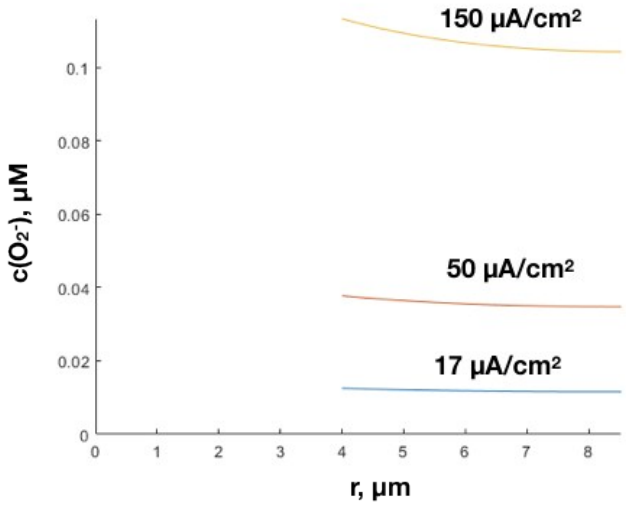

Figure. S4. A steady state superoxide concentration profiles around a carbon fiber at discharge current densities: 150, 50 and 17 μA/cm^2 per electrode geometrical area (superoxide to peroxide conversion rate 0.7 1/s).Д

Li_2O_2 solubility

We used UV-vis spectroscopy of TiO^{2+} complex with H_2O_2 formed in the reaction between dissolved Li_2O_2 and acidic solution of $TiOSO_4$.[2,3] For this purpose, we stirred app. 50 mg of Li_2O_2 in 3 ml of DMSO in glovebox for 1 day. No H_2O_2 was detected after addition of $TiOSO_4$ to filtrated DMSO solution. UV-vis adsorption spectra presented in Fig. 3 show no signal both for dry DMSO and containing 3000 ppm water. It should be noted that the H_2O_2 detection limit in our experiment is $2.6{\cdot}10^{-5}$ M, which is close to $2{\cdot}10^{-5}$ M reported in Ref.[2] Therefore, the equilibrium Li_2O_2 concentration in DMSO with water content less than 3000 ppm is less than $2.6{\cdot}10^{-5}$ M and beyond the detection limit. It is significantly less than the value of $4{\cdot}10^{-4}$ M measured by Ren et al. for dry DMSO.[3] For high water content of 15000 ppm the peak positioned at 408 nm and indicating to the formation of $[Ti(O_2)]^{2+}$ appears in spectrum shown in Fig. S5. The corresponding Li_2O_2 concentration comprises $6{\cdot}10^{-5}$ M.

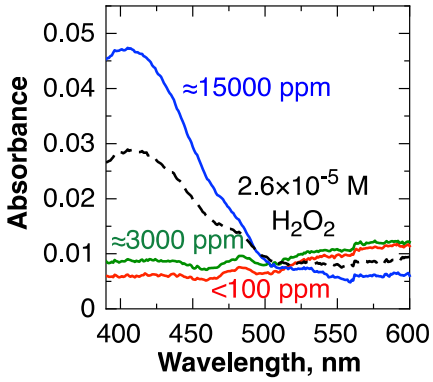

Figure S5. UV-vis adsorption spectra of saturated solutions of Li_2O_2 in DMSO after addition an acidic solution of $TiOSO_4$. $2.6{\cdot}10^{-5}$ M H_2O_2 in DMSO after addition acidic solution of $TiOSO_4$ shown as dashed line.

Estimation of lithium peroxide supersaturation

The diffusion-reaction processes near the flat electrode was modeled numerically to estimate the peroxide concentration that builds up within the above mentioned times. The electrochemical

ORR at the surface is the source of the superoxide specie in the system. Superoxide drains via chemical reaction ($2O_2^- + 2Li^+ \rightarrow Li_2O_2 + O_2$) that at the same time is the source of peroxide. The peroxide drain is absent in this model, as we consider the system evolution before the start of the crystallization process. Such flat electrode model can be described by a simple system of 1-D partial differential equations:

$$\begin{cases} D_1 \dfrac{d^2c_1}{dx^2} - kc_1 = 0 \\ D_2 \dfrac{d^2c_2}{dx^2} + kc_1/2 = 0 \end{cases}$$

where indexes 1 and 2 represents superoxide and peroxide respectively, *D* is diffusion coefficient (both D_1 and D_2 assumed to be 1.1*1e-6 cm^2/s as the latter is unknown), *k* is an effective 1st order rate constant of superoxide to peroxide chemical conversion, *x* – is the distance from the electrode surface.

The boundary conditions are:

$$\left.\frac{dc_1}{dx}\right|_{x=0} = -i/(FD_1); \left.\frac{dc_1}{dx}\right|_{x=+\infty} = 0$$

$$\left.\frac{dc_2}{dx}\right|_{x=0} = 0; \left.\frac{dc_2}{dx}\right|_{x=+\infty} = 0$$

where, *i* is current density and *F* is Faraday constant.

The peroxide concentration profiles presented in Fig. S6 and time evolution concentration near surface is Fig. 4 in main text for k= 24.6 M/s.[4]

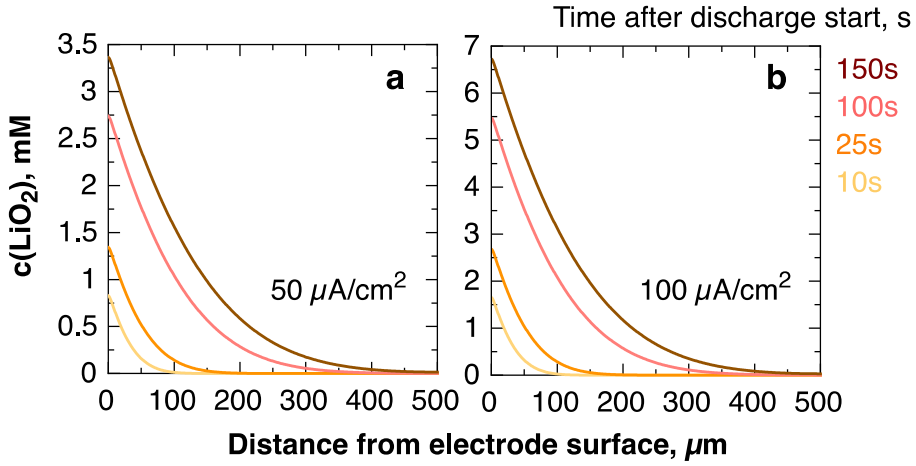

Figure S6. Time evolution of solvated peroxide concentration profiles near the flat electrode surface at 50 μA/cm² (a) and 100 μA/cm² (b)

The peroxide concentration profiles presented in Fig. S7 for k= 0.7 M/s.[5]

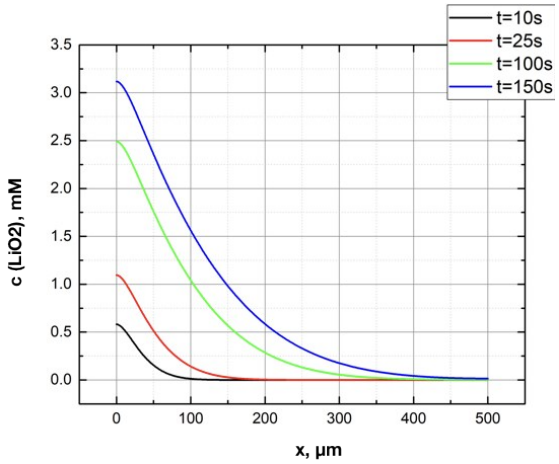

Figure S7. Time evolution of solvated peroxide concentration profiles near the flat electrode surface at 50 µA/cm^2, assuming reaction rate constant k = 0.7 1/s.

Experimental conditions for morphology studies

In order to study structural features and shape of the mesocrystals (or partial mesocrytals) first we should adjust proper discharge conditions, which yield large and spatially separated lithium peroxide particles freely grown on carbon fibers or in the nearest environment. Among key parameters defining morphology we can easily vary the depth of discharge and electrolyte humidity. Our choice is illustrated in Fig. S9. For the fixed water content of 3000 ppm the deep discharge (till abrupt voltage drop) results in complete coverage of electrode surface with unavoidable interplay between particles (Fig. S9c). After 70% discharge some of the particles can be distinguished and analyzed in their shape (Fig. S9b), however they are still strongly influenced by environment. For this reason, in our investigation is focused on electrodes discharged up to 20% of full capacity (Fig S9a). The variation of typical morphology of electrodes discharged to 20 % at different water content is presented in Fig. S9d-f. Similar to the previous observation,[2] the mean particle size is strongly dependent on water content. Note that an increase in the water content leads also to a lower population the surface. Therefore, we consider relatively high water content of about 3000 ppm as most suitable for the observation of mesocrystal morphology. Meanwhile at the lower water content (50 and 500 ppm) smaller and more densely packed particles are observed, that makes harder to extract structural information.

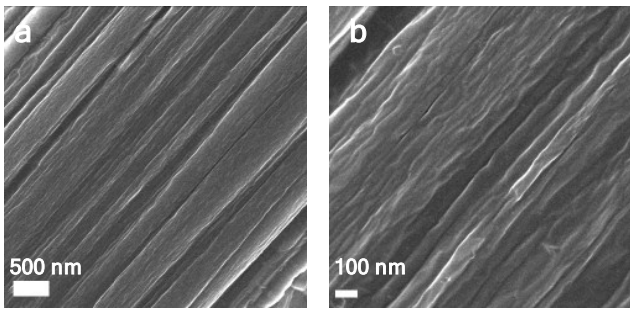

Figure S8. SEM image of pristine electrode – carbon paper TGP-H-90– obtained at different magnifications.

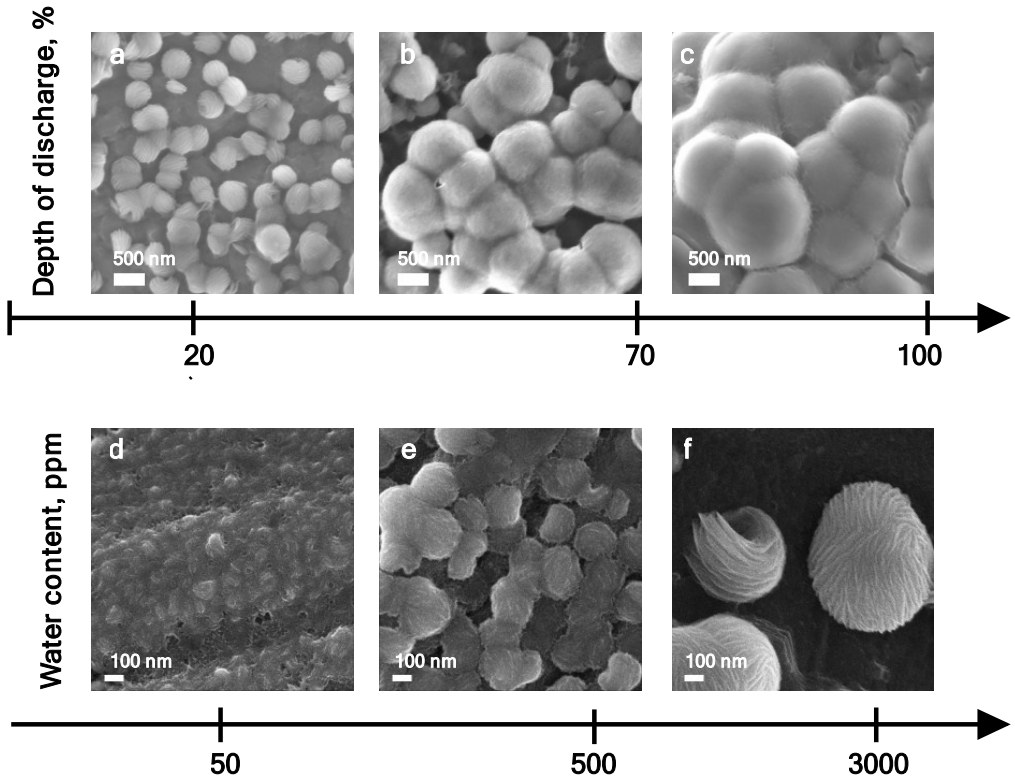

Figure S9. Choice of experimental conditions for morphology studies: a-c) microphotographs obtained for the different discharge depth at water content of 3000ppm H_2O for 20% discharge; d-e) microphotographs obtained for the different water content in electrolyte for the discharge depth of 20%.

Calculation fraction of peroxide on electrode surface

Electrode surface A:

$$A = V(1-\varepsilon)\frac{L'}{S} = V(1-\varepsilon)\frac{2\pi r}{\pi r^2} = \frac{2V(1-\varepsilon)}{r}$$

where $\varepsilon = 0.78$ – electrode porosity, L' – fiber length, S – fiber cross-sectional area, V - electrode volume:

$$V = \frac{\pi h D^2}{4}$$

where D=19.1 mm – electrode diameter, h=280 μm – electrode thickness

Li_2O_2 particles on electrode were approximated as hemispheres with diameter (d) received from size distribution (Fig. S9 c,d).

Number of particles N:

$$N = \left(\frac{2\sqrt{A}}{d}\right)^2$$

Li_2O_2 particle amount – ν_{part}:

$$\nu_{part} = \frac{m}{M_{Li_2O_2}} = \frac{N\rho_{Li_2O_2}V'}{M_{Li_2O_2}} = \frac{N\rho_{Li_2O_2}\pi d^3}{12M_{Li_2O_2}}$$

where m – mass of Li_2O_2, $\rho_{Li_2O_2} = 2.31$ g/cm3 – Li_2O_2 density, $M_{Li_2O_2} = 46$ g/mol – molar mass, V' - volume of 1 hemisphere.

Amount of Li_2O_2 produced during discharge – ν_{dish}:

$$\nu_{dish} = \frac{q}{2F}$$

Where q – cell capacity, F – Faraday constant.

Parameters of calculation and results for two cells are listed in table S1.

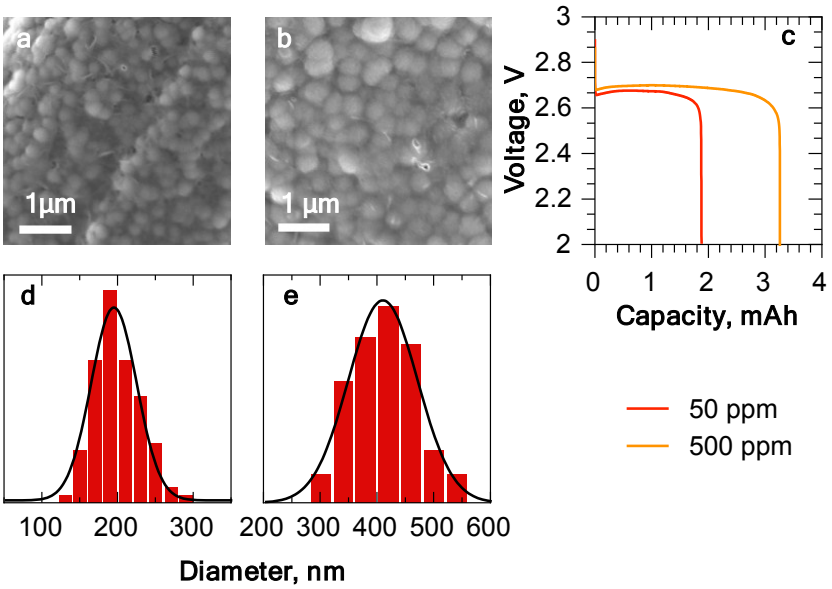

Figure S10. Microphotographs of electrode after full cell discharge at 50 µA/cm2 in 1M LiTFSI in DMSO with water content (a) 50 ppm, (b) 500 ppm water. (c,d) corresponding toroids radial size distribution. (c) discharge curves for these cells.

Table S1. Discharge capacity, particle diameter amount of Li_2O_2 during discharge and Li_2O_2 particles.

Initial water content, ppm	Discharge capacity (q), mAh	Particle diameter (d), nm	ν_{disch}, µmol	ν_{part}, mol
50	1,86	200	3,46	2,49
500	3,39	410	6,32	5,12

Change of X-ray scattering during nucleation

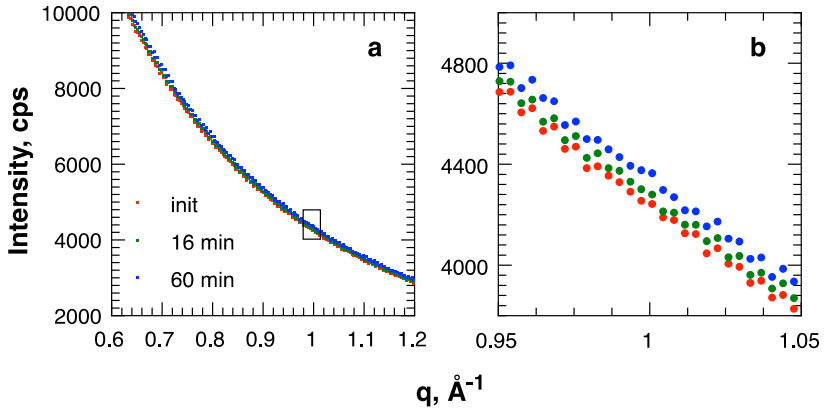

Figure S11. Initial SAXS curve (a) and after corresponding discharge steps (b) for electrochemical cell discharged at -200 µA. Electrode material – carbon fiber paper Toray TGP-H-90

Table S2. SLD[7] and density of compounds and density used in this work.

Compound	ρ, g/cm^3	SLD × 10^5, Å^{-2}
C	2.36	1,87
DMSO (C_2H_6SO)	2.2	1,01
Li_2O_2	1.1	1,93

Table S3. $\Delta\rho^2$ for various interfaces.

Compound 1	Compound 2	$\Delta\rho^2$ × 10^{11}, Å^{-4}
C	DMSO	7,35
C	Li_2O_2	0,03
DMSO	Li_2O_2	8,39

Electrode scattering intensity before discharge I_{init}:[6]

$I_{init} \sim \Delta\rho^2 S_{fX}$

where S_{fX} – electrode surface illuminated by X-rays (spot size $d_X = 1$ mm)

$$S_{fX} = \frac{\pi h d_X^2 (1 - \varepsilon)}{2r}$$

Scattering intensity after formation of nucleus I_{nucl}:

$I_{nucl} \sim \Delta\rho^2 (S_{fX} + S_{nucl})$

where S_{nucl} – surface of all nucleus. Since $\Delta\rho^2$ for C – DMSO and Li_2O_2 – DMSO are close:

$$\frac{I_{nucl}}{I_{init}} = \frac{S_{fX} + S_{nucl}}{S_{fX}}$$

$$S_{nucl} = S_{fX}\left(\frac{I_{nucl}}{I_{init}} - 1\right)$$

Number of nucleus – N_{nucl}:

$$N_{nucl} = \frac{S_{nucl}}{S^*} = \frac{4S_{nucl}}{\pi d^{*2}}$$

where S^* — surface of one nuclei and $d^* = 3$ nm – its diameter.

Nucleus concentration — c_{nucl}:

$$c_{nucl} = \frac{N_{nucl}}{V_{eX}} = \frac{4N_{nucl}}{\varepsilon\pi d_X^2 h} = 5 \times 10^{14}\, particle/cm^3$$

where V_{eX} — electrolyte volume illuminated by X-rays.

Distance between nucleus – l_{nucl}:

$$l_{nucl} = c_{nucl}^{-\frac{1}{3}}$$

Amount of LiO_2 ($\nu^*_{LiO_2}$) in volume for 1 nuclei – V_{nucl}:

$$\nu^*_{LiO_2} = c_{LiO_2} \times V_{nucl} = c_{LiO_2} \times \ {l_{nucl}}^3 = 5 \times 10^{-21}\, mol$$

Amount of Li_2O_2 ($\nu^*_{Li_2O_2}$) in 1 nuclei:

$$\nu^*_{Li_2O_2} = \frac{m^*}{M_{Li_2O_2}} = \frac{\pi {d^*}^3 \rho_{Li_2O_2}}{6 M_{Li_2O_2}} = 7 \times 10^{-22}\, mol$$

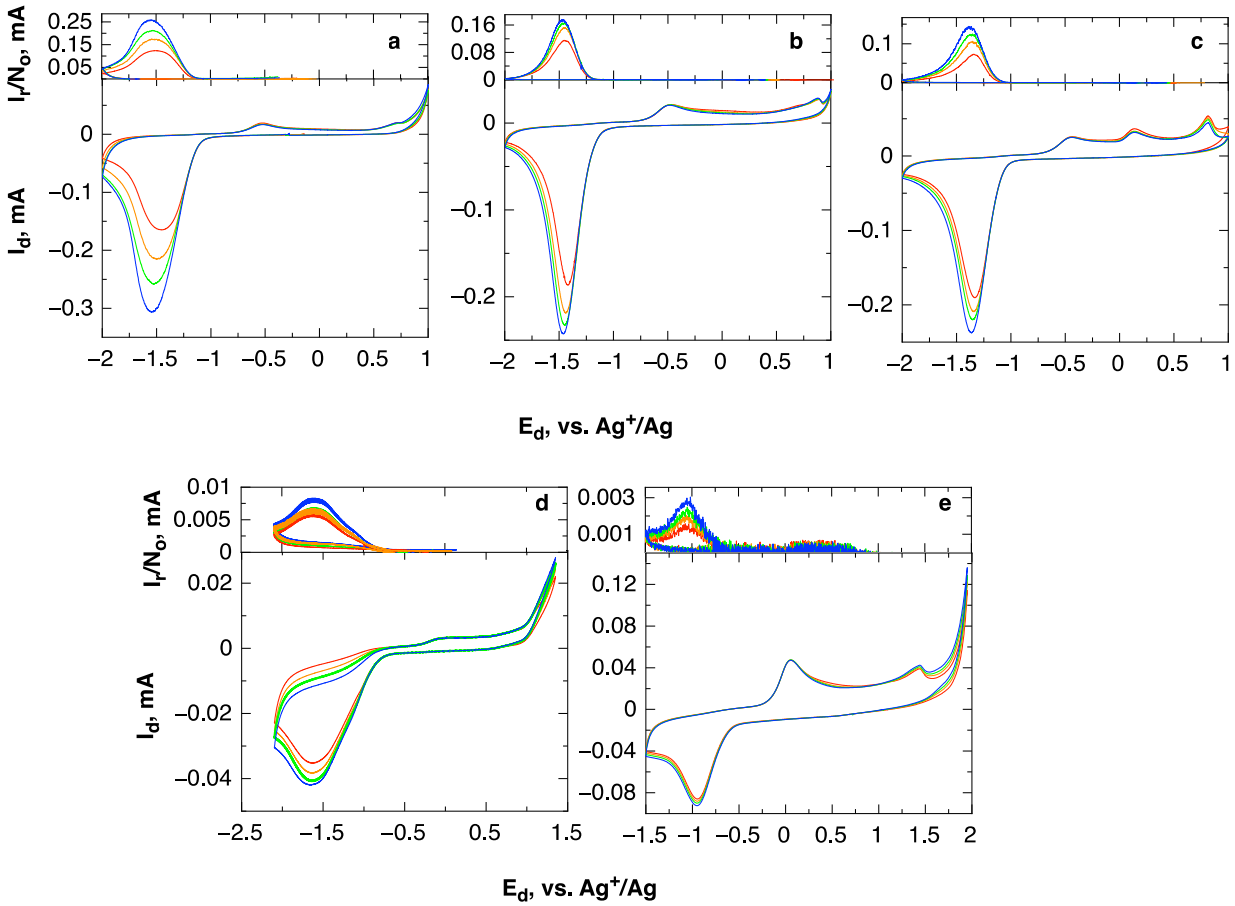

Figure S12. Cyclic voltammetry for GC disk/ Pt ring at 50 mV/s in O_2 saturated 0.1 M $LiClO_4$ in DMSO (a), DMA(b), DMF (c), TEGDME (d), MeCN (e). Rotation speed 1800 rpm.

(1) Itkis, D. M.; Krivchenko, V. A.; Kozmenkova, A. Y.; Pakhotina, M. S.; Napolskiy, F. S.; Gigli, L.; Plaisier, J.; Khasanova, N. R.; Antipov, E. V. Extended Limits of Reversible Electrochemical Lithiation of Crystalline V_2O_5. *CHEMELECTROCHEM* **2019**, *6*, 2013–2019.

(2) Schwenke, K. U.; Metzger, M.; Restle, T.; Piana, M.; Gasteiger, H. A. The Influence of Water and Protons on Li_2O_2 Crystal Growth in Aprotic Li-O_2 Cells. *J. Electrochem. Soc.* **2015**, *162*, A573–A584.

(3) Ren, J.; Huang, Z.; Kalambate, P. K.; Shen, Y.; Huang, Y. Rotating-Disk Electrode Analysis of the Oxidation Behavior of Dissolved Li_2O_2 In Li–O_2 Batteries. *RSC Adv.* **2018**, *8*, 28496–28502.

(4) Zhang, Y.; Zhang, X.; Wang, J.; McKee, W. C.; Xu, Y.; Peng, Z. Potential-Dependent Generation of O_2^- And LiO_2 And Their Critical Roles in O_2 Reduction to Li_2O_2 In Aprotic Li–O_2 Batteries. *J. Phys. Chem. C* **2016**, *120*, 3690–3698.

(5) Johnson, L.; Li, C.; Liu, Z.; Chen, Y.; Freunberger, S. A.; Ashok, P. C.; Praveen, B. B.; Dholakia, K.; Tarascon, J.-M.; Bruce, P. G. The Role of LiO_2 Solubility in O_2 Reduction in Aprotic Solvents and Its Consequences for Li-O_2 Batteries. *Nature Chemistry* 2014, *6*, 1091–1099.

(6) Feigin, L. A.; Svergun, D. I. Structure Analysis by Small-Angle X-Ray and Neutron Scattering. 1987.

(7) SLD Calculator https://sld-calculator.appspot.com (accessed 28 November 2019)